Available online at www.sciencedirect.com
SCIENCE DIRECT®
Journal of Organometallic Chemistry 690 (2005) 895–909
Journal of Organometallic Chemistry
www.elsevier.com/locate/jorganchem

Copolymerization of ethylene/unsaturated alcohols using nickel catalysts: effect of the ligand on the activity and comonomer incorporation

Susete Fernandes [a], Ana Soares [a], Francisco Lemos [b,*], M.A.N.D.A. Lemos [b], João F. Mano [c], Richard J. Maldanis [d], Marvin D. Rausch [d], James C.W. Chien [d,e,f], Maria M. Marques [a,*]

[a] *Centro de Química Estrutural, Instituto Superior Técnico, Av. Rovisco Pais, 1049-001 Lisboa, Portugal*
[b] *Centro de Engenharia Biológica e Química, Instituto Superior Técnico, Departamento de Engenharia Química, Av. Rovisco Pais, 1049-001 Lisboa, Portugal*
[c] *Departamento de Engenharia de Polímeros, Universidade do Minho, Campus Azurém, Guimarães, Portugal*
[d] *Department of Chemistry, University of Massachusetts at Amherst, Amherst MA 01003, USA*
[e] *Department of Polymer Science and Engineering, University of Massachusetts, Amherst MA 01003, USA*
[f] *Amherst Polymer Technology, Inc., 15 Coach Lane, Amherst 01002, USA*

Received 14 May 2004; accepted 16 October 2004
Available online 21 November 2004

Abstract

The nickel complexes {bis[*N*,*N*′-di(2-*t*-butylphenyl)imino]acenaphthene} dibromonickel (**1**-$NiBr_2$) and {bis[*N*,*N*′-di(2-phenylphenyl)imino]acenaphthene} dibromonickel (**2**-$NiBr_2$) were studied in homo-, co- and terpolymerization of ethylene and propylene with polar monomers and the results compared to those previously obtained with another catalyst precursor [bis(*N*,*N*′-dimesitylimino)acenaphthene] dibromonickel (**3**-$NiBr_2$). In order to understand the effect of the ligand in the activity and rate of comonomer incorporation some theoretical studies, using both a semi-empirical molecular orbital method and a density-functional theory model, were performed. Good agreement was found between the computed parameters and the experimental results for the order of homo-polymerization, the differences in polymer molecular weight distribution, and, in some cases, the incorporation of functionalized copolymers in the case of copolymerization, and also on the inhibition effects caused by these copolymers.

Keywords: Copolymerization; Polar monomers; Ni catalysts; Theoretical calculations; Ethylene; Propylene; Cyclic voltammetry

1. Introduction

Ethylene/propylene/α-olefin co- and terpolymers have outstanding chemical resistance and permeability properties. However, they are lacking in adhesion, dyebility and compatibility with additives or more polar polymers. All these properties can be improved by incorporation of functional groups in the hydrocarbon polymer. Commercially available copolymers from ethylene and polar comonomers, mainly from vinyl acetate, acrylic and methacrylic acid and their derivatives are synthesized by radical polymerization at elevated temperature and pressure [1]. Direct insertion of a polar monomer in a polyolefin chain is not possible by heterogeneous Ziegler–Natta catalysts which is attributed to the Lewis acidity of the metal center. However, some pioneering work on direct copolymerization of α-olefins

* Corresponding authors. Tel.: +351 21 8419613; fax: +351 21 8464455.
E-mail addresses: jcwchien@comcast.net (J.C.W. Chien), pci011@mail.ist.utl.pt (M.M. Marques).

0022-328X/$ - see front matter © 2004 Elsevier B.V. All rights reserved.
doi:10.1016/j.jorganchem.2004.10.033

with monomers containing functional groups using homogeneous metallocene-type catalysts has been reported recently [2–4]. In particular, the cationic Ni and Pd complexes with bulky diimine ligands show much improved tolerance against polar functionality [5–8] due to the typically lower Lewis acidity of late transition metals.

The central purpose of this research is to understand the effect of the structure of the ligand in the activity and comonomer incorporation of unsaturated alcohols in their co- and terpolymerization with ethylene and propylene using α-diimine Ni catalysts. Several papers had been published on our work [4,5], the new achievement is the development of theoretical framework for comparisons of polymerization behaviours listed above for Ni catalysts with different ligands.

Theoretical calculations have been used increasingly to elucidate the steps involved in the polymerization and copolymerization processes [9–14].

2. Experimental

2.1. Materials

{Bis[*N*,*N*′-di(2-*t*-butylphenyl)imino]acenaphthene}-dibromonickel, 2^{t}BuPhNiBr$_2$ (**1**-NiBr$_2$), {bis[*N*,*N*′-di-(2-phenylphenyl)imino]acenaphthene}dibromonickel, 2PhPhNiBr$_2$ (**2**-NiBr$_2$) and [bis(*N*,*N*′-dimesitylimino)-acenaphthene]dibromonickel, MesNiBr$_2$ (**3**-NiBr$_2$) were synthesizedaccording to a modified literature procedure [15–20]. 5-Hexen-1-ol (**H**) and 10-undecen-1-ol (**U**) were purchased from Aldrich and degased before being used. Methylaluminoxane (MAO) was supplied by Akzo Chemical Co. Trimethylaluminium (TMA), tri(isobutyl)aluminium (TIBA) and diethylaluminum chloride (DEAC) were obtained from Aldrich.

The electrochemical grade [Bu$_4$N][BF$_4$] electrolyte used in the electrochemical measurements was obtained from Fluka. Dichloromethane was dried and distilled under nitrogen prior to use as solvent.

2.2. Electrochemistry and magnetochemistry

Cyclic voltamograms were obtained using a Radiometer (Model DEA 101) Digital Electrochemical Analyzer interfaced with a Radiometer IMT 102 Electrochemical Interface. The equipment was controlled by a computer, which was also used to acquire the data. All samples were studied in a [Bu$_4$N][BF$_4$]/CH$_2$Cl$_2$ electrolyte solution using a Pt disc (∅ = 1 mm) working electrode in a three-electrode glass cell.

The solution was purged with nitrogen prior to each cyclic voltammogram. All potentials are referred to the [Fe(η^5-C$_5$H$_5$)$_2$]$^{0/+}$ redox couple (0.54 V versus SCE), which was used as an internal standard, and were measured at a scan rate of 200 mV/s.

Magnetic susceptibilities of one of the parent compounds, both in solid state and in solution, were measured using a Gouy Balance (Stanton Model SM.12 with a Newport Instruments $1\frac{1}{2}''$ electromagnet Type C).

2.3. Polymerization

The polymerization apparatus, co- and terpolymerization procedures and polymer work up were described in previous papers [4,21,22].

The polar monomers were treated in situ with TMA or TIBA 5 min before the introduction of the cocatalyst, MAO, and the catalyst precursor. The results were compared to those obtained without using trialkylaluminum as passivating agent.

2.4. Polymer characterization

Homo- and copolymers were analyzed by NMR as described previously [4,8]. ^{1}H and ^{13}C NMR spectra were obtained on samples dissolved in a mixture of 1,2,4-trichlorobenzene with 35% C$_6$D$_6$ at 110 °C or CDCl$_3$ at room temperature. The instrument used was a Varian Unity 300 spectrometer. The internal reference is provided by hexamethyldisiloxane (δ ^{1}H 0.06, δ ^{13}C 1.9 relative to tetramethylsilane) or tetramethylsilane.

Some polymer samples were fractionated using a Soxhlet apparatus. The solvents used were methanol and *n*-heptane. Three fractions were recovered; one insoluble in hot *n*-heptane, another soluble in hot *n*-heptane, which precipitates on cooling down, and a third one soluble in cold *n*-heptane. The fractions were also analyzed by NMR.

The thermal properties of the homo- and copolymers were determined by Differential Scanning Calorimetry (DSC). The equipment used for the DSC analyses was a Perkin–Elmer DSC 7.

2.5. Molecular modelling calculations

Molecular modelling calculations were performed using PC Spartan Pro and PC Spartan 04, for PM3 and DFT calculations. Both programs were supplied by Wavefunction, Inc. and the methods applied are described in the relevant literature [23].

Full geometry optimizations, for all the complexes under analysis, were performed using the PM3 model. Enthalpies of formation of all compounds were also computed under this approximation.

Energy calculations, on these geometries, were computed using an hybrid HF/DFT B3LYP/6-31G** model, which includes a non-local gradient correction.

Most of the calculations were done using a restricted Hartree–Fock approximation (RHF), although some

calculations were also done to estimate the relative energies of triplet states using an unrestricted approximation (UHF).

In order to ascertain the most stable geometry for the parent complexes, full geometry optimizations were performed for **3**-$NiBr_2$ using a LSDA/pBP86/DN* DFT model in PC Spartan Pro, using a square quadrangular geometry for the singlet state and a tetrahedrical geometry for the triplet state.

3. Results and discussion

3.1. Theoretical calculations

The structures of the bis-imino ligands are shown in Fig. 1, where **1**, **2** and **3** have *t*-butylphenyl, phenylphenyl and mesityl substituent, respectively. The heats of formation were computed using both the PM3 semi-empirical molecular orbital method and the B3LYP/6-31G** hybrid HF/DFT model. All structures were fully geometry-optimized, departing both from square planar and tetrahedral initial guesses and using PM3.

3.2. Singlet versus triplet configuration

The kind of nickel complexes that are analyzed in this paper are expected to have either a square-quadrangular geometry, with a singlet electron configuration, or a distorted tetrahedral geometry, in which case a triplet electron configuration is to be expected.

The basic molecular model used for geometry optimization in this paper was the semi-empirical PM3, and the energies were computed, for all the parent compounds, for the singlet and triplet configurations. For all cases the singlet configuration, which always converged to a square-planar geometry, presented the lowest energy value (by about 39.6 kcal/mol for **3**-$NiBr_2$), indicating that it would be the most stable species. The same order is obtained for energies calculated, for these geometries, using the hybrid HF/DFT B3LYP/6-31G** model (the triplet state being 38.0 kcal/mol higher than the singlet one for **3**-$NiBr_2$).

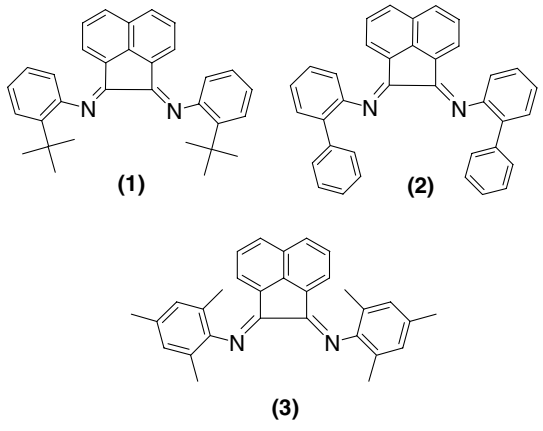

Fig. 1. Schematic representation of the bis-imino ligands **1**, **2** and **3**.

This aspect is particularly relevant for the remainder of this study, since it will indicate which is the parent species that has to be considered for the catalytic cycle.

In order to support the results obtained from the PM3 geometry optimizations, a full geometry optimization was performed using a LSDA/pBP86/DN* DFT model for the (**3**-$NiBr_2$) parent compound. These calculations indicated that the tetrahedral triplet configuration is about 6.95 kcal/mol higher in energy than the square-planar singlet configuration, a value which is considerably lower than the one obtained by PM3, and indicates the possibility of an equilibrium existing between the two species, but still confirms that the square planar is more stable than the tetrahedral one.

We may rationalize the higher energy for the tetrahedral geometry (with a triplet configuration) by the sterical hinderance that the bulky ligands may impose on the two bromide atoms bonded to the nickel and thus, more so, for the other species involved in the catalytic cycle, which have ligands which are still bulkier than the bromides in the parent compounds.

3.3. Species involved in the catalytic cycle

Geometry and energy were obtained for the parent Ni dibromide complexes (**1**-$NiBr_2$, **2**-$NiBr_2$, **3**-$NiBr_2$), the Ni methyl bromide complexes (**1**-NiBrMe, **2**-NiBrMe, **3**-NiBrMe), the unsaturated Ni Me cations (**1**-$NiMe^+$, **2**-$NiMe^+$, **3**-$NiMe^+$), the π-ethylene (E) coordinated Ni methyl cation (**1**-$NiEMe^+$, **2**-$NiEMe^+$, **3**-$NiEMe^+$), the corresponding complexes having one E already inserted in the polymer chain (**1**-$NiPr^+$, **2**-$NiPr^+$, **3**-$NiPr^+$), the corresponding complexes after the next ethylene molecule has been coordinated (**1**-$NiEPr^+$, **2**-$NiEPr^+$, **3**-$NiEPr^+$) and the unsaturated Ni pentyl cation (**1**-$NiPe^+$, **2**-$NiPe^+$, **3**-$NiPe^+$).

This set of species provides a complete view of the energetics of the first few steps in the activation, initiation and propagation reaction, which can be outlined as follows for the family of compounds originating from X = **1**, **2**, **3** (Scheme 1).

The values for the enthalpy of formation for the parent compounds are referred to the following formal reaction (X = **1**, **2**, **3**):

$$X + NiBr_2 \rightarrow [XNiBr_2]$$

and are given in Table 1.

In order to compute the enthalpy associated with this reaction the enthalpy of formation of $NiBr_2$, as well as of the three different ligands **1**, **2** and **3**, were also computed with the same approximations.

The geometry and the enthalpy of formation of the intermediate Ni complexes **1**-NiBrMe, **2**-NiBrMe and

$XNiBr_2 \xrightarrow{MAO} XNiMeBr$ Activation

$XNiMeBr \xrightarrow{MAO} [XNiMe]^+$ Initiation

$[XNiMe]^+ + C_2H_4 \leftrightarrows [XNiEMe]^+$ Coordination

$[XNiEMe]^+ \rightarrow [XNiPr]^+$ Insertion

$[XNiPr]^+ + C_2H_4 \leftrightarrows [XNiEPr]^+$ Coordination

$[XNiEPr]^+ \rightarrow [XNiPe]^+$ Insertion

Scheme 1.

3-NiBrMe, obtained by reaction with MAO by replacing a bromine with a methyl group, were also computed using the same quantum models. The values for the enthalpy are given for the following formal reaction, where $AlMe(OH)_2$ is used as a model for MAO:

$$[XNiBr_2] + AlMe(OH)_2 \rightarrow [XNiMeBr] + AlBr(OH)_2$$

and the values are also given in Table 1. As before, the enthaplies of formation of all the species involved were computed to the same approximation.

The results in Table 1 show that the three neutral α-diimine Ni di-bromide compounds have similar stability. Although the absolute values computed by the two models, PM3 and B3LYP/6-31G** are considerably different, as it would be expected since PM3 is known not to give very reliable absolute energy values, although it gives good estimates of the geometry [13,23], the relative order is the same.

The complex with the ligand **1** seems to have a slightly less negative energy of complex formation, a fact that may be due to the steric constraints that are imposed by this very bulky substituent, and the one with the ligand **2** is clearly the most stable one.

However, if we observe the energy involved in the substitution of a bromine ligand by a methyl group (formation of the methyl-bromine complex), the order is somewhat different; in this case the most favoured complex is the one with ligand **1**. For the other two complexes the two quantum models supply different results. While in the PM3 semi-empirical calculations the least favoured formation should be the one with ligand **2**, DFT calculations, which are supposedly more accurate, indicate that the formation of **3**-NiBrMe is the less exothermic, although the difference between them is not very large.

It is also relevant that both the HOMO and the LUMO for these complexes do not significantly involve the metal atom (as it is depicted in Fig. 2 for the case of complex **2**-$NiBr_2$); the HOMO, which will be involved in the oxidation processes, is mainly centered on the bromine atoms and on the diimine ligand, while the LUMO, which will be involved in the reduction processes, is mainly located on the nitrogen atoms in the diimine ligand and on the carbon atoms of the acenaphtene group nearer to these two nitrogen atoms.

In Table 2, we have computed values of structural and energetic parameters for all the relevant steps in Scheme 1.

The values obtained are in the same order of grandeur of those found in the literature for model compounds for this type of catalysts [12].

The DFT results indicated that the coordination step on the complex that has already a propyl chain, is more favoured for the species with ligand **2** (from **2**-$NiPr^+$ to **2**-$NiEPr^+$ $\Delta H_{Coor.}(C_2H_4) \approx -23.3$ kcal/mol), followed by the one with ligand **3** (from **3**-$NiPr^+$ to **3**-$NiEPr^+$ $\Delta H_{Coor.}(C_2H_4) \approx -11.9$ kcal/mol) and, finally by the one with ligand **1** (from **1**-$NiPr^+$ to **1**-$NiEPr^+$ $\Delta H_{Coor.}(C_2H_4) \approx -11.7$ kcal/mol). The first coordination is more favourable for the species with ligand **3**. PM3 values, however, consistently favour coordination on the complex with ligand **3**.

The fact that the coordination for the complex with ligand **1** is always disfavoured in relation to the other two may be attributed to the bulkyness of the *t*-butyl groups.

A different picture is obtained if one looks at the energy involved in the insertion step. Here, the values obtained for the cases where ligands **1** and **3** are used are quite similar (ca. −14 kcal/mol for the insertion into the propyl chain), while the value for the complex with ligand **2** is somewhat higher than for the other two (less than 1 kcal/mol) for the same insertion. The differences are more important if we look at the process of insertion

Table 1
Energy and geometric parameters for the dibromide α-diimine Ni complexes **X**-$NiBr_2$ and the complexes obtained after the activation step with MAO (**X**-NiBrMe)

Compound	Heat of formation (PM3) (kcal/mol)	Heat of formation (DFT) (kcal/mol)	N–Ni–N angle (°)	HOMO (eV)	LUMO (eV)
1-$NiBr_2$	−222	−96.7	93.00	−4.54	−3.25
2-$NiBr_2$	−226	−96.9	93.16	−5.16	−3.37
3-$NiBr_2$	−227	−101	93.46	−5.10	−3.31
1-NiBrMe	−40.6	−15.1	93.08		
2-NiBrMe	−38.8	−13.3	92.62		
3-NiBrMe	−39.6	−11.7	92.8		

Geometry was optimized at PM3 level and the energy for the formation of the complex was computed by PM3 and by B3LYP/6-31G**. HOMO and LUMO energies were computed at DFT level.

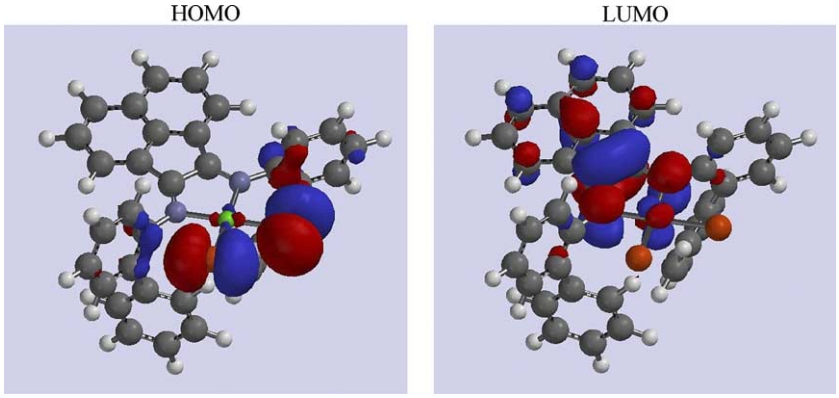

Fig. 2. HOMO and LUMO location in complex **2**-$NiBr_2$, as computed by DFT – B3LYP/6-31G** calculations (see text for details).

Table 2
Structural and energetic parameters for the complexes in Scheme 1

Complex	Distance Ni–C_2H_4 (Å)	Distance Ni–βH (Å)	Chain–ethene angle (°)	$\Delta H_{Coor.}(C_2H_4)$[a] (kcal/mol)		ΔH(insertion) (kcal/mol)	
				PM3	DFT	PM3	DFT
1-$NiEMe^+$	1.925		87.31	−38.9	−20.5		
2-$NiEMe^+$	1.922		87.59	−86.8	−25.6		
3-$NiEMe^+$	1.934		87.58	−75.1	−30.8		
1-$NiPr^+$		1.654				10.3	−2.34
2-$NiPr^+$		1.593				13.7	4.05
3-$NiPr^+$		1.655				10.2	−1.08
1-$NiEPr^+$	1.901		89.95	−48.1	−11.7		
2-$NiEPr^+$	1.892		90.10	−58.7	−23.3		
3-$NiEPr^+$	1.891		89.70	−56.9	−11.9		
1-$NiPe^+$		1.655				20.8	−14.0
2-$NiPe^+$		1.594				32.3	−0.86
3-$NiPe^+$		1.656				29.6	−13.6

Geometry was optimized at PM3 level and the energy for the formation of the complex was computed by PM3 and by B3LYP/6-31G**.

[a] $\Delta H_{Coor.}(C_2H_4)$ was computed as the difference between the heat of formation for the coordination complex and the sum of the heats of formation of complex (**X**-$NiMe^+$ or **X**-$NiPr^+$) and the heat of formation of ethylene computed using the same quantum model.

into the propyl chain. Insertion into the longer chain is around 12 kcal/mol more negative than into the methyl chain, in the cases of the complexes with ligands **1** and **3**; for the complex with ligand **2** the increase in exothermicity is less than 5 kcal/mol. This indicates that there is an increase in chain stabilization as the chain grows, a stabilization which is less important for complexes derived from ligand **2**.

Since insertion is expected to be the rate determining step, and if we take into account the Polanyi principle, this will mean that the energy barrier for the insertion process will increase with the decreased exothermicity/increased endothermicity of the reaction, thus indicating that the rate of polymerization using the complex with ligand **2** will be slower, followed by the one with **3** and then by **1**. This order of reactivity is the same regardless of the model used for the quantum-chemical calculations, although the heat of insertion predicted by the DFT model is negative while PM3 predicts endothermic reactions.

It is interesting to note that the enthalpy involved in the reaction:

$$[XNiPr] + C_2H_4 \rightarrow [XNiPe]$$

should be close to the enthalpy for the gas phase reaction

$$C_3H_6 + C_2H_4 \rightarrow C_5H_{10}$$

the only difference being the change in stability for the coordinated alkyl chain. In fact, as it can be seen in Table 3, the values are quite close for all compounds and all levels of computation. Although the values are quite close, one might notice that the complexes with ligand **2** seems to stabilize less the chain as it grows, since its value is closer to the gas-phase, and re-inforces, the observation made above based on the results for the insertion step.

The geometry of the complexes with the growing chain and an ethylene molecule coordinated can be seen in Fig. 3.

Table 3
Enthalpy (kcal/mol) for the reaction of formation of the pentyl chain on the various complexes, as computed by PM3 and by B3LYP/6-31G** compared to the gas-phase reaction of propylene and ethylene to form 1-pentene

Ligand involved	$\Delta H(C_3H_6 + C_2H_4 \rightarrow C_5H_{10})$	ΔH(Pe–Pr)	
		PM3	DFT
1		−27.3	−25.7
2		−26.4	−24.1
3		−27.3	−25.6
Gas-phase[a]	−22.37		

[a] Computed from values from [24].

The values obtained for the distance between the nickel atom and the β-hydrogen in the growing polymer chain (around 1.65 Å for complexes derived from **1** and **3** and 1.59 Å for the one derived from **2** – see Table 2) are quite close to the value of 1.63 Å found in [12] for a simplified structure for this type of catalyst. It is also interesting to note that this distance is much less in the case of complexes derived from ligand **2** than in the others; should this be the case, this complex would be expected to have a greater participation of β-hydride elimination in the whole process. Thus, polymers obtained with catalysts derived fom ligand **2** are expected to have lower molecular weights than those obtained with any of the other precursors.

In order to analyze the elimination process, geometries and energies for the hydride complexes **1**-NiH$^+$, **2**-NiH$^+$, **3**-NiH$^+$ and for the hydride complexes with an ethylene already coordinated (**1**-NiEH$^+$, **2**-NiEH$^+$, **3**-NiEH$^+$) were also computed. The values obtained are given in Table 4.

The results indicate that the elimination process is highly endothermal and that the energy involved in the simple elimination process

$$[XNiPr]^+ \rightleftharpoons [XNiH]^+ + C_3H_6$$

$$[XNiPe]^+ \rightleftharpoons [XNiH]^+ + C_5H_{10}$$

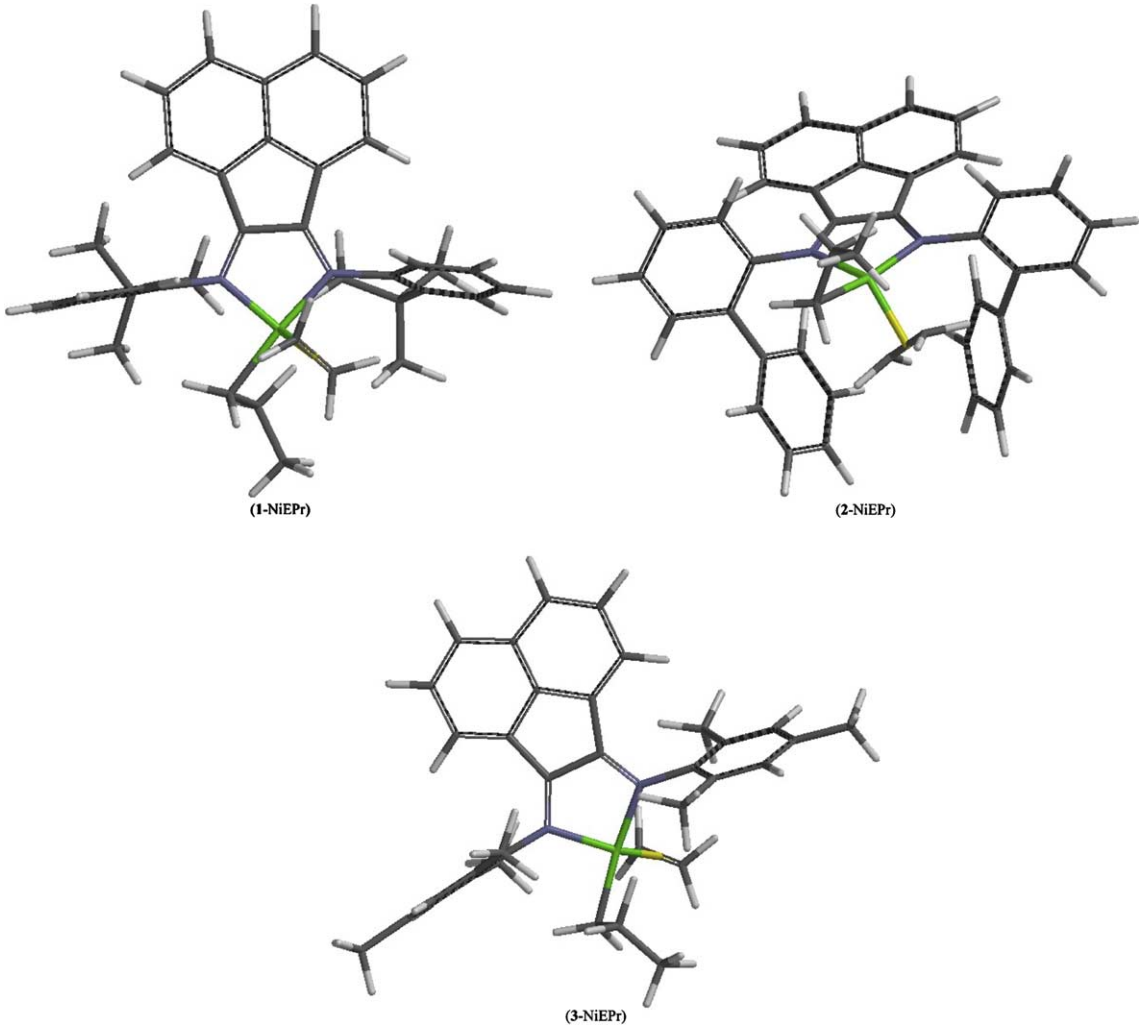

Fig. 3. Geometry of complexes **1**-NiEPr, **2**-NiEPr and **3**-NiEPr, as computed by PM3 calculations (see text for details).

Table 4
Structural parameters for the complexes **X**-NiH$^+$ and **X**-NiEH$^+$ and computed energies for the elimination of the chain

Complex	Distance Ni–C_2H_4 (Å)	Distance Ni–H (Å)	$\Delta H_{1\,\mathrm{Elim.}}$[a] (kcal/mol)		$\Delta H_{2\,\mathrm{Elim.}}$[a] (kcal/mol)	
			PM3	DFT	PM3	DFT
1-NiH$^+$		1.594	42.5	32.5	42.5	34.0
2-NiH$^+$		1.593	96.6	47.2	95.7	47.1
3-NiH$^+$		1.599	107.9	47.1	107.8	48.5
1-NiEH$^+$	1.912	1.593	−3.58	8.32	−3.63	9.81
2-NiEH$^+$	1.921	1.594	−5.80	0.682	−6.74	0.599
3-NiEH$^+$	1.914	1.594	−1.06	11.8	−1.12	13.1

Geometry was optimized at PM3 level and the energy for the formation of the complexes were computed by PM3 and by B3LYP/6-31G**.

[a] $\Delta H_{1\,\mathrm{Elim.}}$ was computed as the difference between the heat of formation for **X**-NiH$^+$ or **X**-NiEH$^+$ added by the heat of formation of propylene and the energy of **X**-NiPr$^+$, added by the heat of formation of ethylene in the case of **X**-NiEH$^+$, computed using the same quantum model. $\Delta H_{2\,\mathrm{Elim.}}$ was computed the same way but using the values for the complex with the pentyl chain and the heat of formation of pentene.

for the propyl and pentyl chains, respectively, is not very dependent on the size of the chain. Apparently, the elimination process is easier in the complexes with **1** and more difficult for the ones with ligand **3**.

However, a different picture is obtained if one looks at the elimination process in a concerted step involving the coordination of one ethylene molecule. This, in fact, seems reasonable since the complex having solely the growing chain, and which is lacking one ligand, is stabilized by the β-agostic hydrogen bond, which supplies the missing ligand. A straightforward elimination would render the complex clearly unsaturated.

However, if one considers the approach of a new ethylene molecule to the unsaturated complex with the growing chain, we can see that for the ethylene to coordinate, either the β-agostic hydrogen bond or the bond to the carbon atom in the growing chain has to be broken. We can then consider the following elimination steps, again for the propyl and pentyl chains

$$[\mathrm{XNiPr}]^+ + \mathrm{Et} \rightleftharpoons [\mathrm{XNiEH}]^+ + \mathrm{C_3H_6}$$

$$[\mathrm{XNiPe}]^+ + \mathrm{Et} \rightleftharpoons [\mathrm{XNiEH}]^+ + \mathrm{C_5H_{10}}$$

If we look at the computed results in Table 4 we can see that this step is much more favourable than the straightforward elimination. In this case, the most favourable elimination process is for the complex with ligand **2**, which is in accordance with the previous observation that the β-agostic hydrogen bond seemed to be stronger for the complexes with this ligand than with the other ones.

If we combine this observation with the one that was previously made that the insertion process was more difficult for the complex with ligand **2** we can say that it is, in fact, expectable that the average molecular weight of the polymer produced with the catalyst based on ligand **2** is lower.

So that a clear picture of the copolymerization process could be obtained, configurations of the complexes with the growing chain (with three carbon atoms in the chain) and 5-hexene-1-ol (**H**) either coordinated (**1**-NiPr**H**$^+$, **2**-NiPr**H**$^+$ and **3**-NiPr**H**$^+$) or already inserted in the polymer chain (**1**-Ni–**H**Pr$^+$, **2**-Ni–**H**Pr$^+$ and **3**-Ni–**H**Pr$^+$) were also geometry-optimized using the PM3 approximation and their energies computed at PM3 and DFT levels. Since there are always many conformations of the chains, both on the alcohol and on the growing chain, several conformations were computed for each complex and the minimum value was used. The results are presented in Table 5.

There is a large difference in the relative values obtained by the semi-empirical and the DFT models.

Table 5
Structural and energetic parameters for the complexes **X**-NiPr**H**$^+$ and **X**-Ni–**H**Pr$^+$

Complex	Distance Ni–**H** (Å)	Distance Ni–βH (Å)	Chain–ethylene angle (°)	$\Delta H_{\mathrm{Coor.}}$(**H**)[a] (kcal/mol)		ΔH (insertion) (kcal/mol)	
				PM3	DFT	PM3	DFT
1-NiPr**H**$^+$	1.94		91.19	−40.5	−8.28		
2-NiPr**H**$^+$	1.92		91.44	59.8	−16.10		
3-NiPr**H**$^+$	1.92		91.65	−157.4	−4.54		
1-Ni–**H**Pr$^+$		1.637				20.56	−9,60
2-Ni–**H**Pr$^+$		1.635				22.60	−6.18
3-Ni–**H**Pr$^+$		1.639				23.02	−7.19

Geometry was optimized at PM3 level and the energy for the formation of the complex was computed by PM3 and by B3LYP/6-31G**.

[a] $\Delta H_{\mathrm{coord}}$(**H**) was computed as the difference between the heat of formation for the complex and the sum of the heats of formation of complex **X**-NiPr$^+$ and the heat of formation of the alcohol (**H**) (−49.386 kcal/mol).

At DFT level the coordination, by the double bond, of the hexenol molecule is always exothermal, although not as much as for the coordination of an ethylene molecule, as it can be seen by comparing the values in Tables 2 and 5. In this case the most favourable situation will be with complex derived from **2**, followed by **1** and then **3**. A very different order is obtained when the calculations are done by the semi-empirical method, in which case the complex derived from **2** is the most disfavoured and **3** is the most favoured.

As for the insertion step, on the other hand, complex with ligand **1** seems to be favoured, although the DFT calculations estimate a slightly exothermic insertion, while PM3 always predicts an endothermic reaction. Complex with ligand **2** is the most disfavoured in the case of DFT calculations and PM3 predicts a higher value for the heat of insertion for the complex derived from **3**.

3.4. Magnetic properties of catalyst precursors

According to the literature, four-coordinate nickel complexes are usually square planar, due to their d^8 configuration. Nickel complexes are usually low-spin and, thus, diamagnetic. Nevertheless, although less common, it is also possible for four-coordinate nickel complexes to assume a distorted tetrahedral geometry and, in general, they will possess high spin; It is also possible that the two isomers, square planar and tetrahedral, exist in equilibrium [25].

As explained above, all geometries that were computed for these catalysts indicate that the most stable configurations for these complexes is a square planar singlet configuration. This is consistent with similar observations found in the literature [12].

However, the solid-state geometry obtained by X-ray diffraction indicated that these complexes have a distorted tetrahedrel geometry [19].

To provide experimental clarification for this issue, the magnetic properties of complex **3**-$NiBr_2$ were measured using a Gouy balance. The magnetic moment was measured in solid state, for which the X-ray diffraction indicated a tetrahedral geometry, and in a 1,2-dichlorobenzene solution.

Solid-state measurement, at 18 °C, gives a molar magnetic susceptibility, of 3.73×10^{-3} cm^3/mol, which yields a magnetic moment of 2.96 Bohr Magnetons and is consistent with a total of two unpaired electrons per molecule.

However, measurement in solution indicated that the compound is diamagnetic. This result was confirmed by NMR measurements, using the Evans method [26,27].

Thus, it seems likely that the complex changes its conformation when dissolved and it will probably exist, in solution, as an equilibrium between the two species, where the diamagnetic species is predominant.

To complement this information some additional molecular modelling calculations were performed using an unrestricted Hartree–Fock approximation (UHF) for triplet states. It was observed that all triplet states also converged to a square planar geometry, regardless of the fact that their initial geometry was set to tetrahedrel, with a significantly higher energy than the singlet state computed under RHF approximation.

3.5. Redox behaviour of catalyst precursors

Complexes **1**-$NiBr_2$, **2**-$NiBr_2$ and **3**-$NiBr_2$ were characterized by cyclic voltammetry. All compounds presented a similar behaviour, which is depicted in Fig. 4 for the case of complex **3**-$NiBr_2$. They all show a

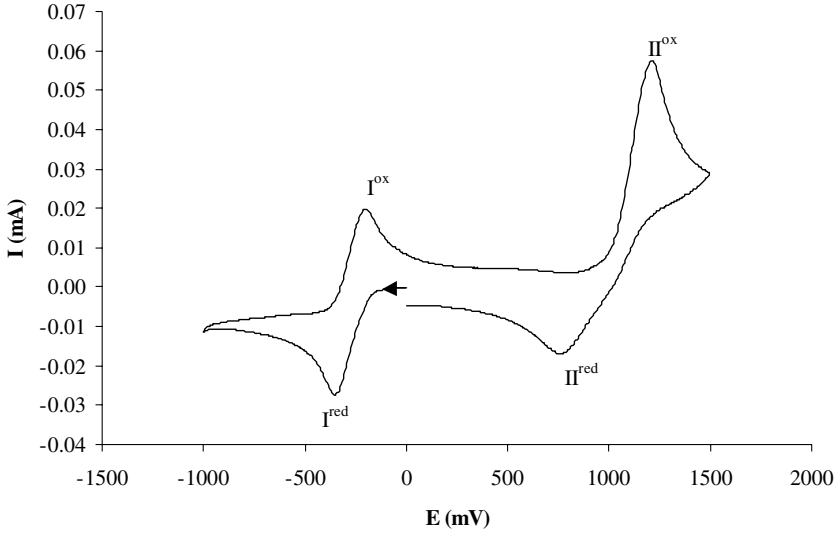

Fig. 4. Cyclic voltammogram of complex **3**, starting with a cathodic sweep, at 200 mV/s (see text for details).

Table 6
Relevant electrochemical data obtained from cyclic voltammetry for **X**-$NiBr_2$

Complex No.	Reduction process (I)			Oxidation process (II)	
	$^{I}E_p^{red}$ (mV)[a]	$^{I}E_p^{ox}$ (mV)[a]	$^{I}E_{1/2}$ (mV)[a]	$^{II}E_p^{ox}$ (mV)[a]	$^{II}E_p^{red}$ (mV)[a]
1-$NiBr_2$	−822	−722	−771	507	
2-$NiBr_2$	−917	−730	−823	550	
3-$NiBr_2$	−840	−730	−785	670	282

[a] Cyclic voltammograms recorded at 200 mV/s, in [Bu4N][BF4]/CH_2Cl_2 electrolyte solution, at a Pt disc electrode. All the potentials values are calculated vs. the FcH/FcH^+ couple.

quasi-reversible reduction wave with a $^{I}E_{1/2}$ around 800 mV (versus the $Fe(C_5H_5)_2/Fe(C_5H_5)_2^+$ redox couple) and an irreversible oxidation wave $^{II}E_p^{ox}$ between 500 and 700 mV, depending on the complex. In the case of complex **3**-$NiBr_2$, upon inversion of the potential cycle after this wave, a cathodic wave appears of much lower intensity than the above-mentioned anodic wave. Table 6 presents the relevant data for these waves for the various compounds.

From these results we can see that complex **2**-$NiBr_2$ is the hardest to reduce, while complex **1**-$NiBr_2$ is the easiest. Comparing the reduction potentials with the values obtained for the energy of the LUMO, one can see that there is no correlation between these values, since the complex which is hardest to reduce, complex **2**-$NiBr_2$, is the one which has the most low-lying LUMO, with an energy of −3.37 eV, and the one that is easiest to reduce has the highest LUMO energy. This lack of correlation occurs both with PM3 computed values (not shown) and with DTF computed ones (values in Table 1), and shows that these methods are probably unreliable method to estimate the values for the energy of these orbitals.

Which orbitals are involved in these electron transfers is unclear. From the quantum-chemical computations it would seem that reduction would be mainly associated with the bi-dentate ligand, where most of the LUMO is located, while the oxidation would mainly involve the bromine ligands, which have most of the electron density associated with the HOMO. However, if we observe the electrochemical behaviour of the acenaphthene ligand, in its free form, we observe that it has a reduction wave at an extremely low potential (−2178 mV for the mesytil-substituted ligand), and an oxidation wave at a potential close to the ones where the complexes also present an oxidation wave (782 mV for the mesityl-substituted ligand). This last fact might imply that the oxidation that is observed for the complexes is mainly associated with the acenaphthene ligand, but this is entirely speculative and is not supported by the quantum-chemical calculations.

It is interesting that, if we look at the energy computed by PM3, in the exchange of a bromine by a methyl (Table 1) we can see that this energy increases (becomes less negative) as the reducibility of the parent compound decreases (the reduction potential becomes more negative). The complex with ligand **2**, being the electronic richer complex, is the one that is more difficult to reduce and consequently where the replacement of a bromide ligand by a methyl ligand is more unfavoured. This may be coincidental, since DFT computed values do not follow this trend.

3.6. Homo-, co- and terpolymerization results

Different cocatalysts were studied in the activation of catalyst precursors **1**-$NiBr_2$ and **2**-$NiBr_2$. Catalyst precursor **3**-$NiBr_2$ has been studied previously [8,28–31] and DEAC had been shown to be one of the best cocatalysts for this system [31]. For the systems where the aniline bears only one substituent group at position 2 such as catalyst precursors **1**-$NiBr_2$ and **2**-$NiBr_2$, TIBA and TMA were found to be very poor cocatalysts. On the other hand, with either MAO or DEAC good activities were achieved by these two catalyst systems in the polymerization of ethylene. MAO was then chosen as cocatalyst in the subsequent studies of **1**-$NiBr_2$ and **2**-$NiBr_2$.

The effect of Al/Ni ratio in the activity of the systems **1**-$NiBr_2$ and **2**-$NiBr_2$ reported in Table 7 shows that the activity of system **1**-$NiBr_2$/MAO in the range of Al/Ni ratios from 300 to 4000 is almost independent of the concentration of MAO. When the concentration of the catalyst **1**-$NiBr_2$ decreases significantly and consequently the ratio Al/Ni increases the activity increases by a factor of about 3.5. This point out either to deactivation of the catalyst due to the formation of dormant sites Ni–E–Ni, which occur at high Ni concentrations or to mass transport limitations. In the case of catalyst **2**-$NiBr_2$ the activity first increases as the ratio Al/Ni increases but for Al/Ni $\geqslant$ 2000 a constant value is obtained.

These results also show that system **1**-$NiBr_2$/MAO is more active than **2**-$NiBr_2$/MAO by a factor of 14. The activity of system **3**-$NiBr_2$/MAO is in between these two values ($A_p = 2.3 \times 10^7$ gPE/molNi · [M] · h) [31], although closer to the **1**-$NiBr_2$ system. These results are in good accordance with the theoretical calculation, both by PM3 and DFT calculations, that indicated that the insertion step should have a larger activation barrier for the complex with ligand **2** followed by **3**, while **1** has the lowest barrier. It is also interesting to note that the coordination step, that is always exothermal, produces

Table 7
Effect of Al/Ni ratio on the activity for ethylene polymerization by the systems **1**-$NiBr_2$ and **2**-$NiBr_2$/MAO

Catalyst system	Run No.	Al/Ni	Activity $\times 10^{-6}$ (gPE/molNi · [M] · h)
1-$NiBr_2$/MAO	R 65[a]	300	9.2
	R 66[a]	500	10.8[d]
	R 67[a]	1000	8.6
	R 69[a]	4000	10.5
	R 93[b]	10000	37.0
	R 92[b]	12000	36.0
2-$NiBr_2$/MAO	RI 6[c]	200	0.4
	RI 83[c]	500	1.7[e]
	RI 9[c]	2000	2.1
	RI 10[c]	4000	2.6

Experimental conditions: $V = 50$ ml toluene; $T = RT$; [E] = 0.35 M.
[a] [Ni] = 62 μM; $t_p = 10$ min.
[b] [Ni] = 0.82 μM; $t_p = 30$ min.
[c] [Ni] = 70 μM; $t_p = 60$ min.
[d] The molecular weight of sample R 66 was measured by GPC and the values obtained were $M_n = 13.2 \times 10^3$ and PD = 4 [19].
[e] The molecular weight of sample RI 83 obtained by NMR was found to be $M_n = 2.2 \times 10^3$. The molecular weight of a sample of PE obtained with the system **3**-$NiBr_2$/MAO under similar experimental conditions, except that a higher Al/Ni was used (Al/Ni = 2200) was found to be higher than that of sample R 66 ($M_n = 41.1$ and PD = 3.5) [8].

a greater stabilization in the case of complex derived from **2** than in the case of the other two (again both by PM3 and DFT calculations), and a smaller one in the case of **1**. Thus, the more important activity of the system using ligand **1** might be linked both to a smaller stabilization of the intermediate complex, with the coordinated olefin molecule, and to the expectable lower activation step in the rate-limiting insertion step.

The average number molecular weight, M_n of polyethylene samples obtained with catalysts precursors **1**-$NiBr_2$ and **3**-$NiBr_2$ is around 10^4 (Tables 7, 10 and 11) while that of samples obtained with the precursor **2**-$NiBr_2$ lie in the range 700–3000 (Tables 7 and 11). This difference, that reaches one to two orders of magnitude, is also consistent with what was expectable based on the theoretical calculations results, that the molecular weight of polymers obtained with the phenyl-substituted precursor **2**-$NiBr_2$ should be lower than those obtained with precursors **1**-$NiBr_2$ and **3**-$NiBr_2$, since the β proton is much closer to the nickel atom in the case of **2**-$NiBr_2$ than with the other two complexes and would, thus, favour the β-elimination reaction. Based on this parameter, the distance between the β-proton and the nickel atom, the elimination step should be of comparable order of magnitude in system based on **1** and **3**, in accordance with experimental values.

All the polymers obtained with these three catalyst systems were shown to be branched polyethylenes. However, the total number of branches and their type are not the same for all the systems (Table 8). The less branched polyethylene samples were obtained with catalyst system

Table 8
Number of branches of polyethylene samples determined by ^{13}C NMR [32]

Type of branches	Catalyst system	Number of branches/1000C		
		1-$NiBr_2$/MAO	**2**-$NiBr_2$/MAO	**3**-$NiBr_2$/MAO [28]
	Run No.	R 199	RI 83	594
Methyl		47	12.5	50.8
Ethyl		10.5	5	7.9
Propyl		–	–	7.3
Butyl		–	7.4	12.8
Amyl		–	–	6.4
Long >5		–	61.3	7.9
Total		57.5	86.2	93.1

1-$NiBr_2$/MAO (57.5/1000C). Systems **2**-$NiBr_2$ and **3**-$NiBr_2$/MAO originate polyethylenes having approximately the same number of branches (around 90/1000C). Besides, in the case of system **1**-$NiBr_2$/MAO only methyl and ethyl branches were observed while in the case of the other systems longer branches were detected. This can be explained according to the bulkiness of the substituent groups of the ligand. It seems that the *t*-Bu group leads to a higher steric hindrance regarding the chain walking process and as a consequence of this, not only the total number of branches is lower, but also the occurrence of long branches is not favoured (mainly methyl branches were formed). When the other two systems are compared, **2**-$NiBr_2$ and **3**-$NiBr_2$/MAO it can be observed that, in spite of the total number of branches being approximately the same, in the case of complex **2**-$NiBr_2$ the occurrence of long branches ($L > 5$) is favoured while mainly methyl branches are observed in the case of complex **3**-$NiBr_2$.

It seems that the phenyl groups in the system based on ligand **2** causes less hindrance than the two *ortho*-methyl substituents in the case of **3**. This has already been observed regarding the β-elimination process since polymers with lower M_n were obtained in the former case than in the latter one.

The activity of the polymerization drops in the presence of unsaturated alcohols even when these are pretreated with alkylaluminium but while in the case of the system **2**-$NiBr_2$/MAO the activity decreases only very slightly, in the case of the other two systems the decrease in the activity is very sharp (Fig. 5).

The concentration of comonomer incorporated in the polymer chain when 5-hexen-1-ol (**H**) and 10-undecen-1-ol (**U**) were copolymerized with ethylene (**E**), using the catalysts systems **1**-$NiBr_2$, **2**-$NiBr_2$ and **3**-$NiBr_2$/MAO are compared in Figs. 6 and 7.

As it can be seen in Fig. 6 the catalyst precursor **3**-$NiBr_2$ shows the best **H** incorporation values [8] followed by **1**-$NiBr_2$. Much smaller incorporation values were found for **2**-$NiBr_2$. In all these experimental runs,

Table 9
Thermal properties of E/**H** and E/**U** copolymers obtained with the catalyst systems **1**-$NiBr_2$/MAO and **2**-$NiBr_2$/MAO

Run No.	Catalyst system	Comonomer/[H] or [U] (mM)	T_{ons} (°C)	ΔH_f (J/g)	T_{ons} (°C)	ΔH_f (J/g)
R 69	**1**-$NiBr_2$/MAO[a]	–	86.5	56.1	96	nd
R 201		**H**/100	84.1[c]	70.3	–	–
R 189		**H**/200	83.1[c]	73.9	–	–
R 203		**H**/300	74.5	66.9	103	nd
R 76		**U**/100	81[d]	37.4	–	–
R 77		**U**/200	59.7[d]	41.3	–	–
R 196		**U**/300	46.3	12.5	99	nd
RI 83	**2**-$NiBr_2$/MAO[b]	–	52.2	44.3	86	nd
RI 99		**H**/100	47.7	109.6	110.4	26
RI 100		**H**/200	56.7[d]	48	–	–
RI 140		**H**/300	47.9	111.4	112.7	18.6
RI 97		**U**/100	47.1	71.2	–	–
RI 131		**U**/200	46	50	114.5	nd
RI 101		**U**/300	64.4	36.5	107	14.1

Experimental conditions: V = 50 ml toluene, T = RT, [E] = 0.35 M. nd, not determined.
[a] [Ni] = 5 μM, t_p = 180 min, Al/Ni = 12000.
[b] [Ni] = 50 μM, t_p = 60 min, Al/Ni = 4000 and Al/Ni = 500 for R 83.
[c] Broad bimodal peak.
[d] Broad peak.

Table 10
Copolymerization of P with **H** and **U** by using the systems **1**-$NiBr_2$ and **3**-$NiBr_2$/MAO

Catalyst system	Run No.	Comonomer/[H] or [U] (mM)	Activity × 10^{-5} (g/molNi · [P] · h)	Polymer OH (mol%)
1-$NiBr_2$/MAO[a]	R 206	–	3.3	–
	R 213	**H**/50	0.6	1
	R 214	**H**/100	0.6	2
	R 228	**H**/200	0.4	3
	R 215	**U**/50	0.9	2
	R 216	**U**/100	0.4	5
	R 229	**U**/200	0.5	6
3-$NiBr_2$/MAO[b]	521 I	–	5.2[c]	–
	521 H	**H**/50	3.3	1
	521 J	**H**/100	0.8	3
	521 K	**H**/200	0.4	4
	521 E	**U**/50	5.3	1
	521 F	**U**/100	1.4	5
	521 L	**U**/200	0.4	8

Experimental conditions: V = 50 ml toluene, T = RT, [P] = 0.69 M.
[a] [Ni] = 10 μM, t_p = 180 min, Al/Ni = 12000.
[b] [Ni] = 42 μM, t_p = 60 min, Al/Ni = 2000.
[c] The molecular weight of sample 521 I was measured by GPC and the values obtained were $M_n = 93.0 \times 10^3$ and PD = 1.7.

the catalyst precursors were activated by MAO and **H** was protected with TMA.

Fig. 7 shows that once more the highest values of comonomer incorporation were obtained with the catalyst precursor **3**-$NiBr_2$ [8] and the lowest ones were obtained with **2**-$NiBr_2$ when the polar monomer used was **U**. No polymer could be obtained when homopolymerizations of **H** and **U** with these catalyst systems were performed. The same happened when no passivating agent was used in the copolymerization.

The results of DSC analysis of the PE, E/**H** and E/**U** copolymers obtained with the catalyst systems **1**-$NiBr_2$ and **2**-$NiBr_2$/MAO are shown in Table 9. Two peaks are observed in the DSC of polyethylene samples obtained with these catalyst systems meaning that two fractions with different morphological units, showing different degrees of crystallinity, are present. The copolymer samples show a similar behaviour since either two separate peaks or a very broad one are observed.

The copolymers E/**H** and E/**U** obtained with the catalyst system **1**-$NiBr_2$/MAO show generally slightly lower onset temperatures than the polyethylene. This is an expected result since the presence of the polar comonomer introduces some disorder in the polymer chains. In fact, T_{ons} decreases as the comonomer incorporation increases. However, in the case of the catalyst system

Table 11
Terpolymerization of E/P with **H** and **U** by using the systems **1**-$NiBr_2$, **2**-$NiBr_2$ and **3**-$NiBr_2$/MAO

Catalyst system	Run No.	Comonomer/[H] or [U] (mM)	E/P	Activity $\times 10^{-6}$ (g/molNi · h)	Polymer OH (mol%)
1-$NiBr_2$/MAO[a]	R 227	–	4/1	2.4	–
	R 225	**H**/50		1.7	0.8
	R 226	**H**/100		1.6	1.1
	R 224	**U**/50		1.6	1.3
	R 223	**U**/100		1.1	2.0
2-$NiBr_2$/MAO[b]	RI 184	–	4/1	0.4[d]	–
	RI 187	**H**/100		0.2[d]	0.1
	RI 188	**U**/50		0.2	0.4
	RI 189	**U**/100		0.2	0.6
3-$NiBr_2$/MAO[c]	180	–	4/1	1.95	–
	168	**H**/50		0.4	1.1
	169	**H**/100		0.4	2.2
	172	**U**/50		0.4	3.7
	173	**U**/100		0.4[e]	5.5

Experimental conditions: $V = 50$ ml toluene, $T = RT$.
[a] [Ni] = 26 μM, $t_p = 90$ min, Al/Ni = 5400.
[b] [Ni] = 66 μM, $t_p = 60$ min, Al/Ni = 4000.
[c] Values reported in [8].
[d] The molecular weight of samples RI 184 and RI 187 obtained by NMR were $M_n = 1.4 \times 10^3$ and 7.4×10^2, respectively.
[e] The molecular weight of sample 173 was measured by GPC and the values obtained were $M_n = 43.0 \times 10^3$ and PD = 3.2.

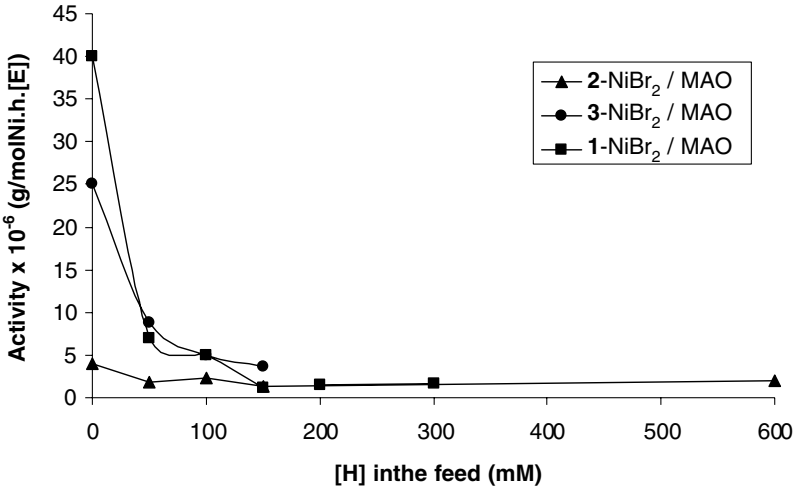

Fig. 5. Activity of polymerization in the presence of 5-hexen-1-ol/TMA.

2-$NiBr_2$/MAO, this effect is not so clear due probably to the low cristallinity shown by the polyethylene itself.

Since the copolymers obtained with **1**-$NiBr_2$ and **2**-$NiBr_2$/MAO systems present a bimodal DSC curve some of them were fractionated using methanol and *n*-heptane. No PE could be isolated by solvent extraction of the product of the reaction. The NMR analysis of these fractions shows that, in all of them, copolymer has been obtained. This fractionation procedure only led to different molecular weight fractions.

Copolymerization of propylene, **P** with the polar monomers **H** and **U** was also studied. The polymerization of **P**, in the absence of alcohol, with the catalyst system **2**-$NiBr_2$/MAO shows an activity of 1.1×10^3 gPP/molNi · [P] · h, the activity is one order of magnitude higher for the system **2**-$NiBr_2$/DEAC ($A_p = 5.3 \times 10^4$ gPP/molNi · [P] · h). The polypropylene obtained is atactic and low molecular weight ($M_w = 1.3 \times 10^3$). This is compared with the propylene homopolymer obtained with the systems **1**-$NiBr_2$/MAO and **1**-$NiBr_2$/DEAC which have $M_w = 35 \times 10^3$ and 49×10^3, respectively [19]. In the presence of the polar monomers **H** and **U** either unprotected orprotected by TMA or just using DEAC/Bu_2Mg, no polymer could be obtained with either the system **2**-$NiBr_2$/MAO or **2**-$NiBr_2$/DEAC. Activities of 3.3×10^5 and 2.5×10^5 gPP/molNi · [P] · h were obtained in the polymerization of **P** using catalyst systems **1**-$NiBr_2$/MAO and **1**-$NiBr_2$/DEAC, respectively; these results compare quite well to those reported in the literature [19] (0.9×10^5 gPP/molNi · [P] · h for

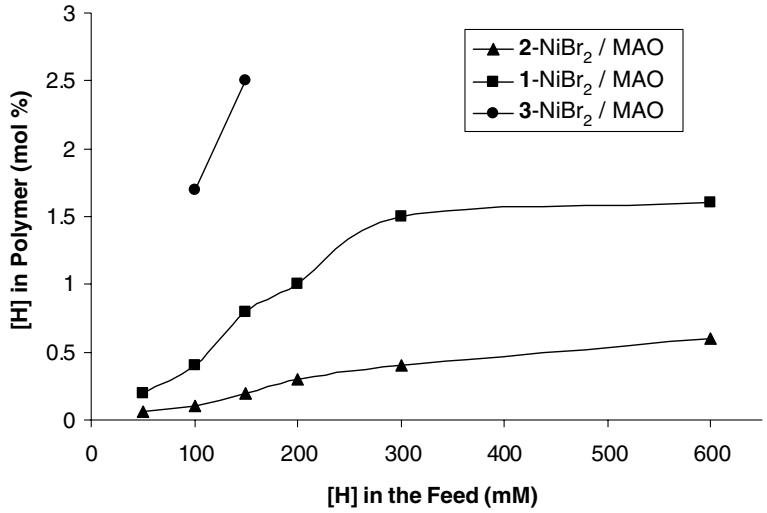

Fig. 6. Concentration of 5-hexen-1-ol incorporated in **E/H** copolymer. **H** was protected with TMA.

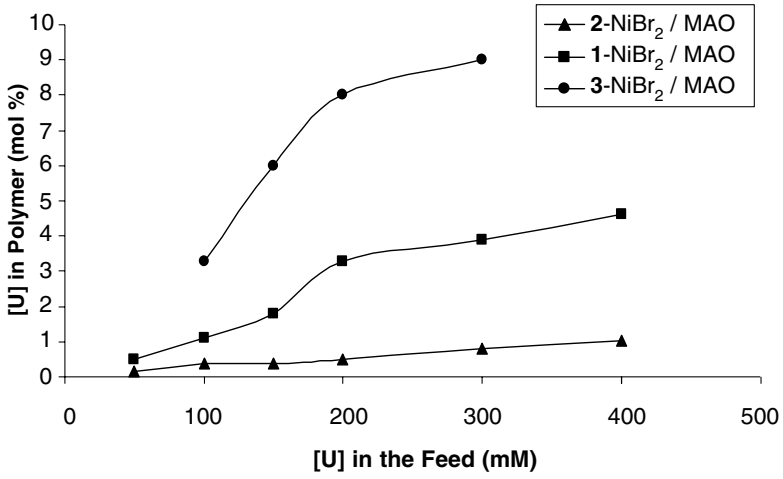

Fig. 7. Concentration of 10-undecen-1-ol incorporated in **E/U** copolymer. **U** was protected by TMA.

system **1**-$NiBr_2$/MAO, and 3.3×10^5 gPP/molNi · [P] · h for system **1**-$NiBr_2$/DEAC). Although the values of the activity of the homopolymerization of **P** are quite similar for both cocatalysts, MAO and DEAC, when comonomers **H** and **U** are used only the system **1**-$NiBr_2$/MAO was found to be active. No polymer could be obtained when DEAC was used as cocatalyst in the copolymerizations of **P/H** and **P/U**. The activity of **P** homopolymerization using the catalyst systems **3**-$NiBr_2$/MAO and **3**-$NiBr_2$/DEAC were reported elsewhere [19,31]. No results of copolymerization of **P** with **H** and/or **U** using catalyst precursor **3** were found in the literature.

Table 10 shows the results obtained in the copolymerization of **P** with polar monomers **H** and **U** using catalyst precursors **1**-$NiBr_2$ and **3**-$NiBr_2$. It can be seen that, for both catalyst systems, the rise of comonomer concentration in the feed leads to an increase of its concentration in the polymer obtained and to a rapid drop in the polymerization activity, as was observed above for the ethylene copolymerization. The comonomer incorporation levels in the polymer obtained with catalyst system **3**-$NiBr_2$/MAO and **1**-$NiBr_2$/MAO are quite similar. However, as observed before, these values are higher in the case of 10-undecen-1-ol than in the case of 5-hexen-1-ol.

The results in Table 11 show that the best activities obtained in terpolymerization reactions were found to be those of catalyst system **1**-$NiBr_2$/MAO while the best incorporation levels were obtained with the system **3**-$NiBr_2$/MAO. Catalyst system **2**-$NiBr_2$/MAO shows the lowest terpolymerization activities and the lowest incorporation values of comonomer similarly to what was found for copolymerization reactions.

Quantum chemical calculations supply two different views in this respect.

Let us look at the results obtained by PM3.

The theoretical results indicate that the coordination of the functionalized alkene is very endothermic in the

case of **2**-$NiBr_2$ (see Table 5), and should, thus, result in very little occupation of the active sites with this molecule, causing little inhibition and, by the same reasoning, a small amount of incorporation of the polar comonomer in the polymer chains, a fact which is consistent with experimental data.

As for catalysts **1**-$NiBr_2$ and **3**-$NiBr_2$ the calculations indicate that both have a very favourable coordination of the comonomer, which is consistent with the general observation that their activity towards ethylene consumption drops significantly, but it is not clear which order should be observed, since complexes derived from **3** presents a heat of coordination for the polar monomer that is much more negative than the one for ethylene and should, thus, present a more pronounced drop in activity and, eventually, a larger degree of incorporation. The former prediction is not entirely consistent with the experimental results, since a concentration of 50 mM of 5-hexen-1-ol in the feed leads to activities which are only 18%, for complex **1**-$NiBr_2$, and 36%, for complex **3**-$NiBr_2$, of the value observed in the absence of any polar monomer, although the degree of reduction is very dependent on the balance between the two relevant steps, coordination and insertion. The latter prediction is in accordance with experimental results. Values for the transition barriers for the two relevant steps would have to be estimated in order to have a more definitive view.

DFT results cannot be related to the results obtained experimentally in a simple manner.

4. Conclusions

Several interesting observations can be extracted from the results presented in this paper.

It seems clear that relatively interesting polar comonomer incorporations can be achieved with these catalysts and that the influence of the structure of the complex has a large impact, not only on homopolymerization rates but also on copolymerization rates and incorporation levels. Incorporation levels of up to 10% were obtained with catalyst **3**-$NiBr_2$, although large activity drops can be expected, even when the comonomer is protected.

Catalysts **1**-$NiBr_2$ and **3**-$NiBr_2$ were the most active for homopolymerization and the incorporation rate of polar monomers is also higher in the case of catalyst precursors **1**-$NiBr_2$ and **3**-$NiBr_2$ than it is in the case of catalyst precursor **2**-$NiBr_2$. Catalyst precursor **3**-$NiBr_2$ is the one that shows higher incorporation rates.

Another interesting aspect is that theoretical calculations can, in fact, provide an adequate tool to analyze the behaviour of the catalysts. In relation to homopolymerization, both PM3 and DFT results showed that the order of activities follows the computed order of thermicity of the insertion step reaction, **1**-$NiBr_2$ being the more active, followed by **3**-$NiBr_2$ and, finally **2**-$NiBr_2$. This is also the order of reducibility of the precursors, as measured by cyclic voltammetry and the order of thermicity for the formation of the methyl bromine complexes, as computed by PM3.

We should note that, since the objective of this work was to analyze the importance of the ligands structure on the behaviour of the catalyst, no simplifications were made to the composition of the compounds in order to perform the quantum-chemical calculations. Both PM3 and DFT seemed adequate to explain homopolymerization data and it should also be stressed that PM3 is a much less time-consuming method than DFT.

These results are in accordance with the tendency found in the literature [10–13] to consider that quantum-chemical calculations are able to help in the understanding of the processes involved and even on the screening of catalysts.

Quantum chemical calculations for the copolymerization process do not supply a simple rationale for the observations and, in some cases, seem not to be in agreement with these observations, perhaps due to the complexity of the molecules involved and the large number of intra-molecular interactions and conformations that can exist. When the polar comonomer is introduced the number of conformations for the species involved increase dramatically and this complicates the analysis that can be performed.

Another interesting observation is that the activity of the catalyst follows the order of reducibility of the precursor, i.e., the more reducible the catalyst precursor (the less negative the potential value at which the reduction occurs), the higher the activity of the catalytic system.

It is also noteworthy that the computed LUMO energy for the catalyst precursor has no correlation with the observed reduction potential, something that may be due to the inability of the quantum-chemical methods that were used for the molecular calculations to adequately estimate this kind of parameters.

Additional studies, involving a more detailed analysis on the transition states for the various steps involved in the reaction scheme and the use of wider variety of quantum-chemical methods would be interesting to expand the conclusions that were drawn from this study. Molecular modelling studies on systems relevant to light olefin polymerization have been gaining an increased interest in the last few years and their adequate application could lead to the development of computational screening techniques for this kind of catalysts.

Acknowledgements

This work was supported in part by Fundação Luso-Americana para o Desenvolvimento (Project 122/2000),

by Fundação para a Ciência e Tecnologia (Project POCTI 32771/QUI and scholarship BIC to A.M.S.) and by FEDER. S.F is grateful for scholarship BD/21354/99 by Fundação para a Ciência e Tecnologia and FSE. We also appreciate the support of Borealis in polymerization equipment.

Appendix A. Supplementary material

^{13}C NMR spectra of polyethylene obtained by catalyst systems **1**-$NiBr_2$/MAO and **2**-$NiBr_2$/MAO. Supplementary data associated with this article can be found, in the online version, at doi:10.1016/j.jorganchem.2004.10.033.

References

[1] K.W. Doak, in: H.F. Mark (Ed.), Encyclopedia of Polymer Science and Engineering, vol. 6, Wiley, New York, 1986, pp. 386–429.
[2] P. Aaltonen, B. Löfgren, Macromolecules 28 (1958) 5353–5357.
[3] P. Aaltonen, G. Fink, B. Löfgren, J. Seppala, Macromolecules 29 (1996) 5255–5260.
[4] M.M. Marques, S.G. Correia, J.R. Ascenso, A.F.G. Ribeiro, P.T. Gomes, A.R. Dias, P. Foster, M.D. Rausch, J.C.W. Chien, J. Polym. Sci. A 37 (1999) 2457–2464.
[5] L.K. Johnson, C.M. Kilian, S.D. Arthur, J. Feldman, E. McCord, S.J. McLain, K.A. Kreutzer, M.A. Benett, E.B. Coughlin, S.D. Ittel, A. Parthasarathy, D.J. Tempel, M.S. Brookhart, WO 96/23010, 1996; Chem. Abstr. 125 (1996) 222773.
[6] L.K. Johnson, S. Mecking, M. Brookhart, J. Am. Chem. Soc. 118 (1996) 267–268.
[7] S. Mecking, L.K. Johnson, L. Wang, M. Brookhart, J. Am. Chem. Soc. 120 (1998) 888–899.
[8] S.G. Correia, M.M. Marques, J.R. Ascenso, A.F.G. Ribeiro, P.T. Gomes, A.R. Dias, M. Blais, M.D. Rausch, J.C.W. Chien, J. Polym. Sci. A 37 (1999) 2471–2780.
[9] J.C.W. Lohrenz, T.K. Woo, L. Fan, T. Ziegler, J. Organomet. Chem. 497 (1995) 91–104.
[10] A. Michalak, T. Ziegler, Organometallics 20 (2001) 1521–1532.
[11] D.M. Phillipp, R.P. Muller, W.A. Goodard III, J. Storer, M. McAdon, M. Mullins, J. Am. Chem. Soc. 124 (2002) 10198–10210.
[12] L. Deng, P. Margl, T. Ziegler, J. Am. Chem. Soc. 119 (1997) 1094–1100.
[13] V.L. Cruz, A. Muñoz-Escalona, J. Martinez-Salazar, J. Polym. Sci. A 36 (1998) 1157–1167.
[14] S. Mukhopadhyay, S.A. Kulkarni, S. Bhaduri, J. Mol. Struct. (Theochem) 673 (2004) 65–77.
[15] L.K. Johnson, C.M. Killian, M. Brookhart, J. Am. Chem. Soc. 117 (1995) 6414–6415.
[16] H. tom Dieck, M. Svoboda, T.Z. Grieser, Z. Naturforsch. B 36 (1981) 823–832.
[17] M. Svoboda, H. tom Dieck, J. Organomet. Chem. 191 (1980) 321–328.
[18] M.S. Blais, Doctoral Dissertation, University of Massachusetts, Amherst, MA, February, 1996.
[19] R.J. Maldanis, J.S. Wood, A. Chandrasekaran, M.D. Rausch, J.C.W. Chien, J. Organomet. Chem. 645 (2002) 158–167.
[20] R.J. Maldanis, Doctoral Dissertation, University of Massachusetts, Amherst, MA, 2003.
[21] J.C.W. Chien, B.P.E. Wang, J. Polym. Sci. A 26 (1988) 3089–3102.
[22] Z. Yu, M.M. Marques, M.D. Rausch, J.C.W. Chien, J. Polym. Sci. A 33 (1995) 979–987.
[23] W.J. Hehre, A Guide to Molecular Mechanis and Quantum Chemical Calculations, Wavefunction, Inc., Irvine, 2003.
[24] R.H. Perry, D.W. Green, Perry's Chemical Engineers Handbook, seventh ed., McGraw-Hill, New York, 1997, pp. 2–195.
[25] F.A. Cotton, G. Wilkinson, P.L. Gaus, Basic Inorganic Chemistry, third ed., Wiley, New York, 1995, p. 573.
[26] D.F. Evans, J. Chem. Soc. (1959) 2003–2005.
[27] J. Loliger, R. Scheffold, J. Chem. Educ. 49 (1972) 646–647.
[28] M.M. Marques, S. Fernandes, S.G. Correia, J.R. Ascenso, T. Nunes, S.G. Pereira, A.F.G. Ribeiro, P.T. Gomes, A.R. Dias, M.D. Rausch, J.C.W. Chien, Macromol. Chem. Phys. 201 (2000) 2464–2468.
[29] S. Fernandes, M.M. Marques, S.G. Correia, J. Mano;, J.C.W. Chien, Macromol. Chem. Phys. 201 (2000) 2566–2572.
[30] M.M. Marques, S. Fernandes, S.G. Correia, S. Caroco, P.T. Gomes, A.R. Dias, J. Mano, M.D. Rausch, J.C.W. Chien, Polym. Int. 50 (2001) 579–587.
[31] J.C.W. Chien, S. Fernandes, S.G. Correia, M.D. Rausch, L.C. Dickinson, M.M. Marques, Polym. Int. 51 (2002) 729–737.
[32] G.B. Galland, R.F. de Souza, R.S. Mauler, F.F. Nunes, Macromolecules 32 (1999) 1620–1625.